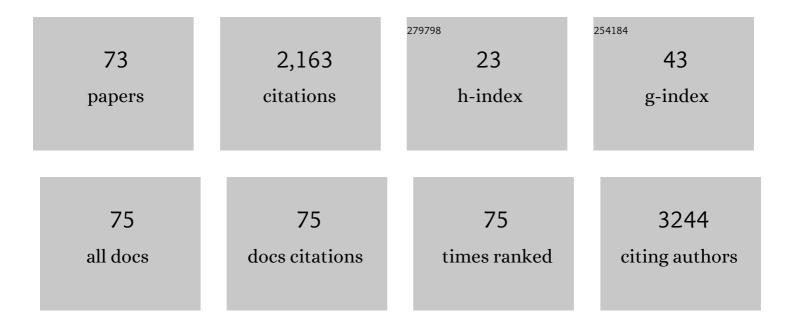
Hai-Ling Margaret Cheng

List of Publications by Year in descending order

Source: https://exaly.com/author-pdf/2746222/publications.pdf Version: 2024-02-01



#	Article	IF	CITATIONS
1	Rapid high-resolutionT1 mapping by variable flip angles: Accurate and precise measurements in the presence of radiofrequency field inhomogeneity. Magnetic Resonance in Medicine, 2006, 55, 566-574.	3.0	296
2	Steady-State MR Imaging Sequences: Physics, Classification, and Clinical Applications. Radiographics, 2008, 28, 1147-1160.	3.3	236
3	Practical medical applications of quantitative MR relaxometry. Journal of Magnetic Resonance Imaging, 2012, 36, 805-824.	3.4	176
4	Investigation and optimization of parameter accuracy in dynamic contrastâ€enhanced MRI. Journal of Magnetic Resonance Imaging, 2008, 28, 736-743.	3.4	95
5	Tissue thermal conductivity by magnetic resonance thermometry and focused ultrasound heating. Journal of Magnetic Resonance Imaging, 2002, 16, 598-609.	3.4	86
6	Temporal resolution and SNR requirements for accurate DCEâ€MRI data analysis using the AATH model. Magnetic Resonance in Medicine, 2010, 64, 1772-1780.	3.0	72
7	T1 measurement of flowing blood and arterial input function determination for quantitative 3DT1-weighted DCE-MRI. Journal of Magnetic Resonance Imaging, 2007, 25, 1073-1078.	3.4	66
8	Complementary Strategies for Developing Gd-Free High-Field <i>T</i> ₁ MRI Contrast Agents Based on Mn ^{III} Porphyrins. Journal of Medicinal Chemistry, 2014, 57, 516-520.	6.4	50
9	Quantification of renal perfusion: Comparison of arterial spin labeling and dynamic contrastâ€enhanced MRI. Journal of Magnetic Resonance Imaging, 2011, 34, 608-615.	3.4	49
10	Accurate liver T measurement of iron overload: A simulations investigation and in vivo study. Journal of Magnetic Resonance Imaging, 2009, 30, 313-320.	3.4	46
11	Quantifying angiogenesis in VEGF-enhanced tissue-engineered bladder constructs by dynamic contrast-enhanced MRI using contrast agents of different molecular weights. Journal of Magnetic Resonance Imaging, 2007, 25, 137-145.	3.4	40
12	A general dual-bolus approach for quantitative DCE-MRI. Magnetic Resonance Imaging, 2011, 29, 160-166.	1.8	39
13	MRI and contrastâ€enhanced ultrasound monitoring of prostate microwave focal thermal therapy: An in vivo canine study. Journal of Magnetic Resonance Imaging, 2008, 28, 136-143.	3.4	38
14	Delayed Gadolinium-enhanced MR Imaging of Articular Cartilage: Three-dimensional T1 Mapping with Variable Flip Angles and B1Correction. Radiology, 2009, 252, 865-873.	7.3	35
15	Normal Tissue Quantitative T1 and T2â^— MRI Relaxation Time Responses to Hypercapnic and Hyperoxic Gases. Academic Radiology, 2011, 18, 1159-1167.	2.5	31
16	Quantitative MRI assessment of VX2 tumour oxygenation changes in response to hyperoxia and hypercapnia. Physics in Medicine and Biology, 2011, 56, 1225-1242.	3.0	30
17	An enzyme-activatable and cell-permeable Mn ^{III} -porphyrin as a highly efficient T ₁ MRI contrast agent for cell labeling. Chemical Science, 2016, 7, 4308-4317.	7.4	29
18	Gadoliniumâ€free <i>T</i> ₁ contrast agents for MRI: Tunable pharmacokinetics of a new class of manganese porphyrins. Journal of Magnetic Resonance Imaging, 2014, 40, 1474-1480.	3.4	27

#	Article	IF	CITATIONS
19	Dynamic contrast-enhanced MRI to quantify VEGF-enhanced tissue-engineered bladder graft neovascularization: Pilot study. Journal of Biomedical Materials Research - Part A, 2006, 77A, 390-395.	4.0	26
20	3D myocardial <i>T</i> ₁ mapping at 3T using variable flip angle method: Pilot study. Magnetic Resonance in Medicine, 2014, 71, 823-829.	3.0	26
21	Improved correlation to quantitative DCEâ€MRI pharmacokinetic parameters using a modified initial area under the uptake curve (mIAUC) approach. Journal of Magnetic Resonance Imaging, 2009, 30, 864-872.	3.4	25
22	Binding of a dimeric manganese porphyrin to serum albumin: towards a gadolinium-free blood-pool T 1 MRI contrast agent. Journal of Biological Inorganic Chemistry, 2014, 19, 229-235.	2.6	25
23	Prediction of subtle thermal histopathological change using a novel analysis of Gd-DTPA kinetics. Journal of Magnetic Resonance Imaging, 2003, 18, 585-598.	3.4	24
24	Dynamic Gd-DTPA enhanced MRI as a surrogate marker of angiogenesis in tissue-engineered bladder constructs: A feasibility study in rabbits. Journal of Magnetic Resonance Imaging, 2005, 21, 415-423.	3.4	23
25	Impact of motion on T1 mapping acquired with inversion recovery fast spin echo and rapid spoiled gradient recalledâ€echo pulse sequences for delayed gadoliniumâ€enhanced MRI of cartilage (dGEMRIC) in volunteers. Journal of Magnetic Resonance Imaging, 2010, 32, 394-398.	3.4	23
26	Ectopic fat in youth: The contribution of hepatic and pancreatic fat to metabolic disturbances. Obesity, 2014, 22, 1280-1286.	3.0	22
27	Monitoring angiogenesis in soft-tissue engineered constructs for calvarium bone regeneration: an in vivo longitudinal DCE-MRI study. NMR in Biomedicine, 2010, 23, 48-55.	2.8	21
28	Ultrashort Echo Time for Improved Positive-Contrast Manganese-Enhanced MRI of Cancer. PLoS ONE, 2013, 8, e58617.	2.5	21
29	A scale to measure MRI contrast agent sensitivity. Scientific Reports, 2017, 7, 15493.	3.3	20
30	A manganese porphyrin-based T1 contrast agent for cellular MR imaging of human embryonic stem cells. Scientific Reports, 2018, 8, 12129.	3.3	19
31	Monitoring tissue development in acellular matrixâ€based regeneration for bladder tissue engineering: Multiexponential diffusion and <i>T</i> ₂ * for improved specificity. NMR in Biomedicine, 2012, 25, 418-426.	2.8	18
32	Liver iron overload assessment by <i>T</i> magnetic resonance imaging in pediatric patients: An accuracy and reproducibility study. American Journal of Hematology, 2012, 87, 435-437.	4.1	18
33	Effect of Hyperoxia and Hypercapnia on Tissue Oxygen and Perfusion Response in the Normal Liver and Kidney. PLoS ONE, 2012, 7, e40485.	2.5	18
34	Dynamic Contrast-Enhanced MRI in Oncology Drug Development. Current Clinical Pharmacology, 2007, 2, 111-122.	0.6	17
35	The acellular matrix (ACM) for bladder tissue engineering: A quantitative magnetic resonance imaging study. Magnetic Resonance in Medicine, 2010, 64, 341-348.	3.0	17
36	A technique for rapid singleâ€echo spinâ€echo <i>T</i> ₂ mapping. Magnetic Resonance in Medicine, 2010, 64, 536-545.	3.0	17

#	Article	IF	CITATIONS
37	and T ₁ assessment of abdominal tissue response to graded hypoxia and hypercapnia using a controlled gas mixing circuit for small animals. Journal of Magnetic Resonance Imaging, 2016, 44, 305-316.	3.4	17
38	A non-invasive magnetic resonance imaging approach for assessment of real-time microcirculation dynamics. Scientific Reports, 2017, 7, 7468.	3.3	17
39	Manganese-porphyrin-enhanced MRI for the detection of cancer cells: A quantitative in vitro investigation with multiple clinical subtypes of breast cancer. PLoS ONE, 2018, 13, e0196998.	2.5	16
40	One‣tep Labeling of Collagen Hydrogels with Polydopamine and Manganese Porphyrin for Nonâ€Invasive Scaffold Tracking on Magnetic Resonance Imaging. Macromolecular Bioscience, 2019, 19, e1800330.	4.1	16
41	Primer and Historical Review on Rapid Cardiac <scp>CINE MRI</scp> . Journal of Magnetic Resonance Imaging, 2022, 55, 373-388.	3.4	16
42	Usefulness of contrast kinetics for predicting and monitoring tissue changes in muscle following thermal therapy in long survival studies. Journal of Magnetic Resonance Imaging, 2004, 19, 329-341.	3.4	15
43	Quantitative Magnetic Resonance Imaging Assessment of Matrix Development in Cell-Seeded Natural Urinary Bladder Smooth Muscle Tissue-Engineered Constructs. Tissue Engineering - Part C: Methods, 2010, 16, 643-651.	2.1	13
44	Concurrent Dual Contrast for Cellular Magnetic Resonance Imaging Using Gadolinium Oxide and Iron Oxide Nanoparticles. International Journal of Molecular Imaging, 2012, 2012, 1-10.	1.3	13
45	Noninvasive Manganese-Enhanced Magnetic Resonance Imaging for Early Detection of Breast Cancer Metastatic Potential. Molecular Imaging, 2014, 13, 7290.2013.00071.	1.4	13
46	Synthesis of degradable-polar-hydrophobic-ionic co-polymeric microspheres by membrane emulsion photopolymerization: In vitro and in vivo studies. Acta Biomaterialia, 2019, 89, 279-288.	8.3	13
47	Next-generation multimodality of nutrigenomic cancer therapy: sulforaphane in combination with acetazolamide actively target bronchial carcinoid cancer in disabling the PI3K/Akt/mTOR survival pathway and inducing apoptosis. Oncotarget, 2021, 12, 1470-1489.	1.8	12
48	The Next-Generation of Combination Cancer Immunotherapy: Epigenetic Immunomodulators Transmogrify Immune Training to Enhance Immunotherapy. Cancers, 2021, 13, 3596.	3.7	12
49	Optimized T1- and T2-weighted volumetric brain imaging as a diagnostic tool in very preterm neonates. Pediatric Radiology, 2011, 41, 702-710.	2.0	11
50	Manganeseâ€enhanced MRI of minimally gadoliniumâ€enhancing breast tumors. Journal of Magnetic Resonance Imaging, 2015, 41, 806-813.	3.4	11
51	Assessment of microvascular dysfunction in acute limb ischemiaâ€reperfusion injury. Journal of Magnetic Resonance Imaging, 2019, 49, 1174-1185.	3.4	11
52	Gadoliniumâ€free extracellular MR contrast agent for tumor imaging. Journal of Magnetic Resonance Imaging, 2015, 41, 397-403.	3.4	10
53	An Efficient <i>T</i> ₁ Contrast Agent for Labeling and Tracking Human Embryonic Stem Cells on MRI. Contrast Media and Molecular Imaging, 2019, 2019, 1-11.	0.8	10
54	MRI method for labeling and imaging decellularized extracellular matrix scaffolds for tissue engineering. Magnetic Resonance in Medicine, 2020, 83, 2138-2149.	3.0	10

#	Article	IF	CITATIONS
55	Bright Ferritin—a Reporter Gene Platform for On-Demand, Longitudinal Cell Tracking on MRI. IScience, 2020, 23, 101350.	4.1	10
56	Human Aortic Endothelial Cell Labeling with Positive Contrast Gadolinium Oxide Nanoparticles for Cellular Magnetic Resonance Imaging at 7 Tesla. Molecular Imaging, 2012, 11, 7290.2011.00037.	1.4	9
57	Positive-contrast cellular MRI of embryonic stem cells for tissue regeneration using a highly efficient <i>T</i> ₁ MRI contrast agent. Journal of Magnetic Resonance Imaging, 2016, 44, 1456-1463.	3.4	9
58	Heart failure with preserved ejection fraction: the missing pieces in diagnostic imaging. Heart Failure Reviews, 2020, 25, 305-319.	3.9	9
59	Establishment of a Lung Metastatic Breast Tumor Xenograft Model in Nude Rats. PLoS ONE, 2014, 9, e97950.	2.5	9
60	Manganese-Enhanced Magnetic Resonance Imaging for Early Detection and Characterization of Breast Cancers. Molecular Imaging, 2014, 13, 7290.2014.00021.	1.4	8
61	3D Multicellular Stem-Like Human Breast Tumor Spheroids Enhance Tumorigenicity of Orthotopic Xenografts in Athymic Nude Rat Model. Cancers, 2021, 13, 2784.	3.7	8
62	UBR4/POE facilitates secretory trafficking to maintain circadian clock synchrony. Nature Communications, 2022, 13, 1594.	12.8	7
63	A novel MRI analysis for assessment of microvascular vasomodulation in low-perfusion skeletal muscle. Scientific Reports, 2020, 10, 4705.	3.3	5
64	Skeletal Muscle Microvascular Dysfunction Manifests Early in Diabetic Cardiomyopathy. Frontiers in Cardiovascular Medicine, 2021, 8, 715400.	2.4	5
65	Fate, complications and MRI implications of retention anchor suture placed during gastrostomy in children. Pediatric Radiology, 2013, 43, 1009-1016.	2.0	4
66	Physiologic characterization of inflammatory arthritis in a rabbit model with BOLD and DCE MRI at 1.5 Tesla. European Radiology, 2014, 24, 2766-2778.	4.5	4
67	Ultrashort Echo Time Magnetic Resonance Imaging of the Lung Using a High-Relaxivity T ₁ Blood-Pool Contrast Agent. Molecular Imaging, 2014, 13, 7290.2014.00027.	1.4	4
68	<scp>USPIO</scp> â€related T1 and T2 mapping <scp>MRI</scp> of cartilage in a rabbit model of bloodâ€induced arthritis: a pilot study. Haemophilia, 2015, 21, e59-69.	2.1	4
69	Human microvascular reactivity: a review of vasomodulating stimuli and non-invasive imaging assessment. Physiological Measurement, 2021, 42, 09TR01.	2.1	4
70	Threeâ€Dimensional Bioprinted <scp>MRâ€Trackable</scp> Regenerative Scaffold for <scp>Postimplantation</scp> Monitoring on <scp>T1â€Weighted MRI</scp> . Journal of Magnetic Resonance Imaging, 2022, 56, 570-578.	3.4	4
71	Microvascular Dysfunction in Skeletal Muscle Precedes Myocardial Vascular Changes in Diabetic Cardiomyopathy: Sex-Dependent Differences. Frontiers in Cardiovascular Medicine, 2022, 9, .	2.4	2
72	Abstract 1220: Investigation of the biological properties of human breast cancer in a nude rat model. ,		0

Abstract 2014, , .

# ARTICLE		
 Abstract 3133: The anti-tumor effects of acetazolamide and sulforaphane on broncl Preclinical modeling and mechanism. , 2014, , . 	chial carcinoids:	0